IET Microwaves, Antennas & Propagation

Research Article

IET Journals
The Institution of Engineering and Technology

Balanced-to-unbalanced power dividers for arbitrary power division ratios and for arbitrary real termination impedances

ISSN 1751-8725
Received on 12th June 2018
Revised 23rd October 2018
Accepted on 12th February 2019
E-First on 15th March 2019
doi: 10.1049/iet-map.2018.5424
www.ietdl.org

Hee-Ran Ahn[1] ✉, *Manos M. Tentzeris*[1]

[1]*The school of Electrical and Computer Engineering, Georgia Institute of Technology, Atlanta, GA 30332, USA*

✉ *E-mail: hranahn@gmail.com*

Abstract: Novel balanced-to-unbalanced power divider (BUPD) is introduced for arbitrary power division ratios and for arbitrary real termination impedances. It consists of one 180° transmission-line section (TL), two different 90° TLs and one isolation circuit comprising two different resistances and two different 90° TLs. Due to the arbitrary termination impedances, the conventional ways for the even- and odd-mode excitation analyses are impossible, requiring a new design method. Under the assumption of the perfect isolation between two output ports, the BUPD can be divided into two, based on which the design formulas for the characteristic impedances of all the TLs can be successfully derived. Then, the scattering parameters are inversely derived, which is quite different from the conventional ways where the design formulas are derived based on the scattering parameters. For the verification of the suggested theory, one prototype for the power division ratio of 5 dB and for the termination impedances of 60, 40 and 50 Ω is tested. The measured frequency responses are in good agreement with the predicted ones.

1 Introduction

A balanced circuit is circuitry commonly used with balanced lines or just the balanced line itself. Balanced lines are a common method of transmitting many types of electrical communication signals between two points on two wires. The two signal lines are of a matched impedance, and the common-mode rejection can be achieved at the receiving end by the balanced circuitry. Applying this principle, balanced filters, balanced diplexers, balanced antennas, and balanced power dividers have demonstrated for good common-mode suppression and high immunity to environmental and device electronic noise.

Various balanced power dividers have been reported since 2012 [1], and different topologies have been introduced for equal power divisions [1–8] or for the arbitrary power divisions [9–12]. The number of single-ended ports of the balanced power dividers is six but it shows that the balanced power dividers function correctly only with four single-ended ports demonstrating the successful common-mode rejection and two unbalanced outputs.

Among those topologies reported in [1–12], the ones listed in [3, 6, 7, 11, 12] suggest balanced-to-unbalanced power dividers (BUPDs) for equal or arbitrary power divisions but the termination impedances are equal or only two of three are different [12]. That is, none of the previous reported geometries has been implemented for arbitrary real termination impedances, a capability that would feature a great advantage for the total size miniaturisation due to the elimination of additional matching circuits [13–22]

To overcome the above shortcomings, here, BUPDs are introduced for arbitrary power division ratios and for arbitrary real termination impedances. The proposed BUPD topology consists of one 180° transmission-line section (TL), two 90° TLs and one isolation circuit which is a novel circuit consisting of two 90° TLs and two different resistances values which are the same as the termination impedances at two unbalanced ports.

However, due to the arbitrary termination impedances, the circuitry is not symmetric and, therefore, the conventional even- and odd-mode excitation analyses cannot be applied. Thus, the design formulas based on the topology are relatively difficult to derive. Instead of the symmetry line, the BUPD can be divided into two under the assumption of the perfect isolation, based on which the design formulas for the characteristic impedances of the TLs can be successfully derived.

To verify the design formulas, one prototype terminated in 60, 40 and 50 Ω is designed and measured at 2 GHz for the power division ratio of 5 dB. The measured responses are in good agreements with the predicted ones.

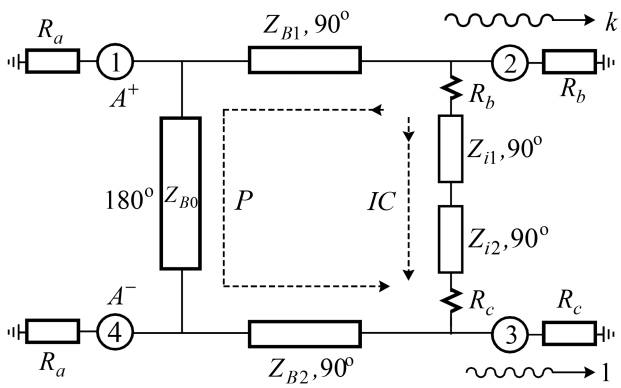

Fig. 1 *BUPD topology*

2 BUPDs (balanced-to-unbalanced power dividers)

The BUPD topology depicted in Fig. 1 is composed of four single-ended ports ①, ②, ③ and ④, the two ports ① and ④ of which form one balanced common port A terminated in R_a, while the other two ports ② and ③ are terminated in R_b and R_c, respectively. The topology in Fig. 1 consists of one 180° TL with the characteristic impedance Z_{B0}, two 90° TLs with the different characteristic impedances of Z_{B1} and Z_{B2} and an isolation circuit (IC). The IC consists of two 90° TLs with the characteristic impedances of Z_{i1} and Z_{i2} and two resistors with the values of R_b and R_c. The power division ratio between ports ② and ③ is k^2 as indicated in Fig. 1. The BUPD is not symmetric and, therefore, conventional even- and odd-mode excitation analyses are not possible.

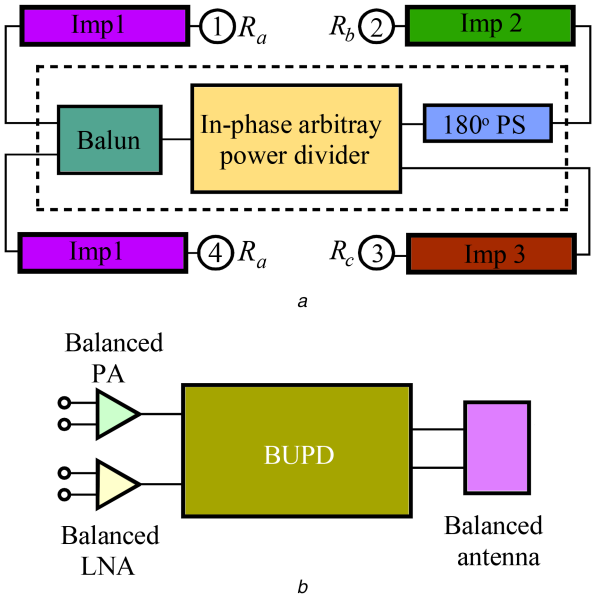

Fig. 2 *Building blocks of BUPD and its application*
(a) BUPD with a PD, a balun, a 180° phase shifter (PS) and four impedance transformers, ***(b)*** A fully balanced RF front end

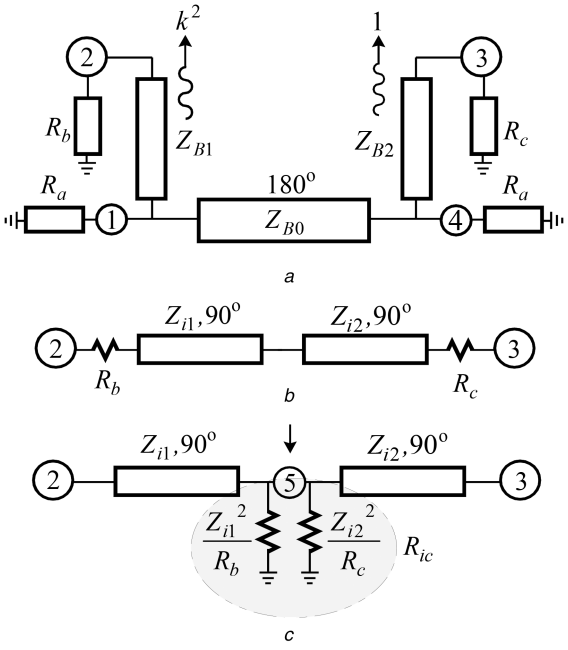

Fig. 3 *P -circuit and IC in terms of ports ② and ③*
(a) *P* -circuit, ***(b)*** *IC*, ***(c)*** *T*- type *IC* equivalent circuit

2.1 Potential applications

The BUPD in Fig. 1 consist of an in-phase PD with arbitrary power divisions, one balun, a 180° phase shifter (180° PS) and four impedance transformers (Imp1, Imp2 and Imp3), two of which are identical as Imp1 as depicted in Fig. 2*a*.

There are no small number of applications of the BUPDs and one of them is a fully balanced RF front end, consisting of a balanced power amplifier (PA), a balanced low noise amplifier (LAN), a BUPD, and a balanced antenna as illustrated in Fig. 2*b*. Two signals of the PA and LNA are connected to the two balanced ports of the BUPD and two output ports are connected to the balanced antenna for wider impedance bandwidth, better cross-polarisations and less sensitivity to the ground perturbation.

2.2 Design formulas

For the BUPD in Fig. 1 to function correctly, the unbalanced ports ② and ③ should be perfectly matched, and a perfect isolation between ports ② and ③ should be achieved at the design frequency, regardless of the common ports ① and ④. Using this concept, the design formulas can be easily derived. Under the assumption of the perfect isolation between ports ② and ③, the BUPD in Fig. 1 can be separated into two circuits, namely, *P* -circuit and *IC*, as illustrated in Fig. 3*a* and *b*, respectively. The *ABCD* parameters of the *P* -circuit and *IC* are in terms of ports ② and ③ given as

$$\begin{bmatrix} A & B \\ C & D \end{bmatrix}_{P\_23} = \begin{bmatrix} 0 & jZ_{B1} \\ j\frac{1}{Z_{B1}} & 0 \end{bmatrix} \begin{bmatrix} 1 & 0 \\ \frac{1}{R_a} & 1 \end{bmatrix} \begin{bmatrix} -1 & 0 \\ 0 & -1 \end{bmatrix} \begin{bmatrix} 1 & 0 \\ \frac{1}{R_a} & 1 \end{bmatrix} \begin{bmatrix} 0 & jZ_{B2} \\ j\frac{1}{Z_{B2}} & 0 \end{bmatrix} \quad (1a)$$

$$\begin{bmatrix} A & B \\ C & D \end{bmatrix}_{IC} = \begin{bmatrix} 1 & R_b \\ 0 & 1 \end{bmatrix} \begin{bmatrix} 0 & jZ_{i1} \\ j\frac{1}{Z_{i1}} & 0 \end{bmatrix} \begin{bmatrix} 0 & jZ_{i2} \\ j\frac{1}{Z_{i2}} & 0 \end{bmatrix} \begin{bmatrix} 1 & R_c \\ 0 & 1 \end{bmatrix} \quad (1b)$$

Using matrix conversion [18], the admittance parameters of the both circuits in Fig. 3*a* and *b* are given as

$$\begin{bmatrix} Y_{11} & Y_{12} \\ Y_{21} & Y_{22} \end{bmatrix}_{P\_23} = \frac{R_a}{2} \begin{bmatrix} \frac{1}{Z_{B1}^2} & -\frac{1}{Z_{B1}Z_{B2}} \\ -\frac{1}{Z_{B1}Z_{B2}} & \frac{1}{Z_{B2}^2} \end{bmatrix} \quad (2a)$$

$$\begin{bmatrix} Y_{11} & Y_{12} \\ Y_{21} & Y_{22} \end{bmatrix}_{IC} = \begin{bmatrix} \frac{1}{R_b + R_c T^2} & \frac{T}{R_b + R_c T^2} \\ \frac{T}{R_b + R_c T^2} & \frac{T^2}{R_b + R_c T^2} \end{bmatrix} \quad (2b)$$

where $T = Z_{i1}/Z_{i2}$.

In the isolation circuit in Fig. 3*b*, the series isolation resistors R_b and R_b can be transformed into the parallel ones as shown in Fig. 3*c* where the transformed values are Z_{i1}^2/R_b and Z_{i2}^2/R_c [21], and the fifth port ⑤ is assumed. When the power division ratio between ports ② and ③ in Fig. 3*a* is k^2, that between ports ② and ③ of the *T*-type *IC* in Fig. 3*c* should be $1/k^2$ [13, 14] with the excitation at port ⑤, leading to the ratio of R_b/Z_{i1}^2 to R_c/Z_{i2}^2 being $1/k^2$. Thus, the ratio of Z_{i1} to Z_{i2} is given as

$$\frac{Z_{i1}}{Z_{i2}} = k\sqrt{\frac{R_b}{R_c}} \quad (3)$$

To simultaneously achieve the perfect matching at ports ② and ③ and the perfect isolation between ports ② and ③, the sum of the admittance parameters of the *P* - circuit and *IC* should be

$$\begin{bmatrix} Y_{11} & Y_{12} \\ Y_{21} & Y_{22} \end{bmatrix}_{P\_23} + \begin{bmatrix} Y_{11} & Y_{12} \\ Y_{21} & Y_{22} \end{bmatrix}_{IC} = \begin{bmatrix} G_b & 0 \\ 0 & G_c \end{bmatrix} \quad (4)$$

where $G_b = R_b^{-1}$ and $G_c = R_c^{-1}$. Substituting (3) into (2b) gives

$$\begin{bmatrix} Y_{11} & Y_{12} \\ Y_{21} & Y_{22} \end{bmatrix}_{IC} = \begin{bmatrix} \frac{1}{(1+k^2)R_b} & \frac{k}{(1+k^2)\sqrt{R_b R_c}} \\ \frac{k}{(1+k^2)\sqrt{R_b R_c}} & \frac{k^2}{(1+k^2)R_c} \end{bmatrix} \quad (5)$$

Using the relations in (4) and (5), the admittance parameters of the *P* - circuit can be expressed as

$$\begin{bmatrix} Y_{11} & Y_{12} \\ Y_{21} & Y_{22} \end{bmatrix}_{P\_23} = \begin{bmatrix} \dfrac{k^2}{(1+k^2)R_b} & -\dfrac{k}{(1+k^2)\sqrt{R_bR_c}} \\ -\dfrac{k}{(1+k^2)\sqrt{R_bR_c}} & \dfrac{1}{(1+k^2)R_c} \end{bmatrix} \quad (6)$$

The characteristic impedances of Z_{B1} and Z_{B2} can be derived from (2a) and (6) as

$$Z_{B1} = \sqrt{\frac{(1+k^2)}{2k^2}}\sqrt{R_aR_b} \quad (7a)$$

$$Z_{B2} = \sqrt{\frac{(1+k^2)}{2}}\sqrt{R_aR_c} \quad (7b)$$

$$Z_{B0};\ \text{arbitrary} \quad (7c)$$

where the characteristic impedance Z_{B0} can be chosen as an arbitrary real value. The admittance matrix of the $T-$ type in Fig. 3*c* is

$$\begin{bmatrix} Y_{11} & Y_{12} \\ Y_{21} & Y_{22} \end{bmatrix}_{T\_IC} = R_{ic}\begin{bmatrix} \dfrac{1}{Z_{i1}^2} & \dfrac{1}{Z_{i1}Z_{i2}} \\ \dfrac{1}{Z_{i1}Z_{i2}} & \dfrac{1}{Z_{i2}^2} \end{bmatrix} \quad (8)$$

where R_{ic} is a parallel connection Z_{i1}^2/R_b and Z_{i2}^2/R_c and expressed as

$$\frac{1}{R_{ic}} = \frac{R_b}{Z_{i1}^2} + \frac{R_c}{Z_{i2}^2} \quad (9)$$

From the other elements in the matrices (2b), (5) and (8), the characteristic impedances of Z_{i1} and Z_{i2} of the *T*-type in Fig. 3*c* are derived as

$$Z_{i1} = \sqrt{(1+k^2)}\sqrt{R_bR_{ic}} \quad (10a)$$

$$Z_{i2} = \sqrt{\frac{(1+k^2)}{k^2}}\sqrt{R_cR_{ic}} \quad (10b)$$

$$R_{ic};\ \text{arbitrary} \quad (10c)$$

where the resistance value of R_{ic} should be realised with a lumped-element resistor and, therefore, can be selected arbitrarily, based on the available chip resistors.

2.3 Scattering parameters

Based on the design formulas in (7a)–(7c) and (10a)–(10c), the standard and mixed scattering matrices of the BUPDs in Fig. 1 will be derived inversely to the conventional ways. For this, the scattering parameters between the balanced ports ① and ④ are required to derive. The topology shown in Fig. 4 is the *P* - circuit viewed from ports ① and ④ where two input impedances of Z_{in2} and Z_{in3} are indicated, which are

$$Y_{in2} = \left(\frac{Z_{B1}^2}{R_b}\right)^{-1} = \frac{2k^2}{(1+k^2)R_a} \quad (11a)$$

$$Y_{in3} = \left(\frac{Z_{B2}^2}{R_c}\right)^{-1} = \frac{2}{(1+k^2)R_a} \quad (11b)$$

where $Y_{in2} = Z_{in2}^{-1}$ and $Y_{in3} = Z_{in3}^{-1}$.

The *ABCD* parameters of the *P* - circuit defined by the network *N* in Fig. 4 are, in terms of ports ① and ④, given by

$$\begin{bmatrix} A & B \\ C & D \end{bmatrix}_{P\_14} = \begin{bmatrix} 1 & 0 \\ Y_{in2} & 1 \end{bmatrix}\begin{bmatrix} -1 & 0 \\ 0 & -1 \end{bmatrix}\begin{bmatrix} 1 & 0 \\ Y_{in3} & 1 \end{bmatrix} \quad (12)$$

Substituting (11a), (11b) into (12) gives

$$\begin{bmatrix} A & B \\ C & D \end{bmatrix}_{P\_14} = -\begin{bmatrix} 1 & 0 \\ \dfrac{2}{R_a} & 1 \end{bmatrix} \quad (13)$$

Using the conversion of *ABCD* into scattering parameters [18], the scattering parameters in terms of ports ① and ④ in Fig. 4 are obtained as

$$\begin{bmatrix} S_{11} & S_{14} \\ S_{41} & S_{44} \end{bmatrix}_{P\_14} = -\frac{1}{2}\begin{bmatrix} 1 & 1 \\ 1 & 1 \end{bmatrix} \quad (14)$$

When only port ① is excited, the unitary property should be satisfied as follows;

$$|S_{11}|^2 + |S_{21}|^2 + |S_{31}|^2 + |S_{41}|^2 = 1 \quad (15)$$

The scattering parameter ratio of S_{21} to S_{31} should be k to realise a power division ratio of k^2 to give

$$\frac{|S_{21}|}{|S_{31}|} = k \quad (16)$$

When either port ① or ④ is excited, the two divided waves at ports ② and ③ are 180° out of phase. Considering the power division ratio (16), the perfect isolation between ports ② and ③ and the perfect matching at ports ② and ③ in (4) as well as the expression (14) of the scattering parameters correlating ports ① and ④, the standard scattering matrix $[S_{std}]$ is derived as

$$[S_{std}] = \begin{bmatrix} S_{11} & S_{12} & S_{13} & S_{14} \\ S_{12} & 0 & 0 & -S_{21} \\ S_{13} & 0 & 0 & -S_{31} \\ S_{14} & -S_{12} & -S_{13} & S_{11} \end{bmatrix} \quad (17)$$

where

$$S_{11} = S_{14} = -\frac{1}{2} \quad (17a)$$

$$S_{12} = -j\frac{k}{\sqrt{2(k^2+1)}} \quad (17b)$$

$$S_{13} = j\frac{1}{\sqrt{2(k^2+1)}} \quad (17c)$$

Based on the standard scattering parameters (17), (17a)–(17c), the mixed-mode scattering matrix $[S_{mm}]$ can be obtained using superposition of balanced and common-mode signals, as well. With the balanced signals, the scattering parameter S_{AA}^{dd} at the common port *A* is determined by S_{11}, S_{44}, S_{41}, and S_{14}, and the scattering

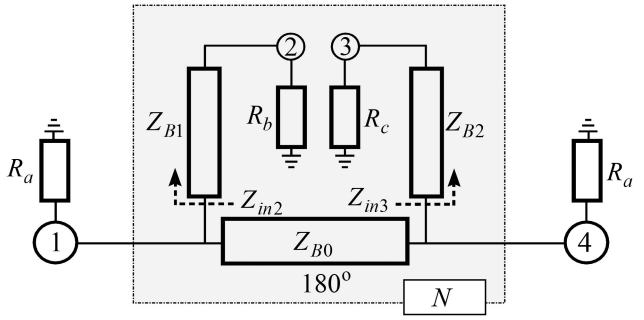

Fig. 4 *P - circuit in terms of ports ① and ④*

parameters S_{2A}^{sd} and S_{3A}^{sd} due to the power transfers from port A to the balanced ports ② and ③, respectively, are determined by S_{21}, S_{24}, S_{31} and S_{34} such as

$$S_{AA}^{dd} = \frac{1}{2}(S_{11} + S_{44} - S_{41} - S_{14}) \tag{18a}$$

$$S_{2A}^{sd} = \frac{\sqrt{2}}{2}(S_{21} - S_{24}) \tag{18b}$$

$$S_{3A}^{sd} = \frac{\sqrt{2}}{2}(S_{31} - S_{34}) \tag{18c}$$

On the other side, assuming common-mode signals at ports ① and ④, the mixed-mode scattering parameters of S_{AA}^{cc}, S_{2A}^{sc} and S_{3A}^{sc} are in a similar way expressed as

$$S_{AA}^{cc} = \frac{1}{2}(S_{11} + S_{44} + S_{41} + S_{14}) \tag{19a}$$

$$S_{2A}^{sc} = \frac{\sqrt{2}}{2}(S_{21} + S_{24}) \tag{19b}$$

$$S_{3A}^{sc} = \frac{\sqrt{2}}{2}(S_{31} + S_{34}) \tag{19c}$$

The scattering parameters of S_{AA}^{dc} and S_{AA}^{cd} at the common ports ① and ④ are

$$S_{AA}^{dc} = \frac{1}{2}(S_{11} - S_{44} + S_{14} - S_{41}) \tag{20a}$$

$$S_{AA}^{cd} = \frac{1}{2}(S_{11} - S_{44} - S_{14} + S_{41}) \tag{20b}$$

Thus, by using the relations in (18a)–(18c) to (20a) and (20b), the mixed-mode scattering matrix $[S_{mm}]$ can be summarised as

$$[S_{mm}] = \begin{bmatrix} S_{AA}^{dd} & S_{A2}^{ds} & S_{A3}^{ds} & S_{AA}^{dc} \\ S_{2A}^{sd} & S_{22}^{ss} & S_{23}^{ss} & S_{2A}^{sc} \\ S_{3A}^{sd} & S_{32}^{ss} & S_{33}^{ss} & S_{3A}^{sc} \\ S_{AA}^{cd} & S_{A2}^{cs} & S_{A3}^{cs} & S_{AA}^{cc} \end{bmatrix} \tag{21}$$

$$= \begin{bmatrix} 0 & -j\frac{k}{\sqrt{k^2+1}} & j\frac{1}{\sqrt{k^2+1}} & 0 \\ -j\frac{k}{\sqrt{k^2+1}} & 0 & 0 & 0 \\ j\frac{1}{\sqrt{k^2+1}} & 0 & 0 & 0 \\ 0 & 0 & 0 & -1 \end{bmatrix}$$

2.4 Discussion about conventional designs

The design parameters of all the conventional BUPDs in [3, 6, 7, 11, 12] are derived based on the given scattering parameters and needed to be compared.

The conventional BUPDs [3] are derived based on the given scattering parameters and can be applied only for equal power division and for equal termination impedances of 50 Ω, while the *T*-type isolation circuit in Fig. 3*c* is adopted. For the case of $k = 1$, $R_a = R_b = R_c = 50\,\Omega$ in Fig. 1 and $R_{ic} = 50\,\Omega$ in Fig. 3*c*, the characteristic impedances of Z_{B1}, Z_{B2}, Z_{i1} and Z_{i2} are, based on (7a)–(7c) and (10a)–(10c), calculated as $Z_{i1} = Z_{i2} = 70.71\,\Omega$ and $Z_{B1} = Z_{B2} = 50\,\Omega$. The two values of $Z_{i1} = Z_{i2} = 70.71\,\Omega$ are the same as those in [3, Sec. II. D], but the two identical 90° TLs with $Z_{B1} = Z_{B2} = 50\,\Omega$ are represented by another additional circuit depicted in Fig. 5*a* where the characteristic impedances are all equal to $Z_3 = 50\,\Omega$ and the electrical lengths are Θ_1, Θ_2 and Θ_3. Their respective four design parameters are listed in Table 1 where groups 1, 2, and 3 are those in [3, Table 1] and the fourth set of data indicated as 'design I' are those for the measurement of the prototype in [3, Fig. 15]. If it is verified that the characteristic impedances and the electrical lengths of the conventional filter in Fig. 5*a* with the given design parameters in Table 1 are 50 Ω and 90°, respectively, the calculation values from (7a)–(7c) and (10a)–(10c) can be the same as those in [3] for $k = 1$ and $R_a = R_b = R_c = 50\,\Omega$.

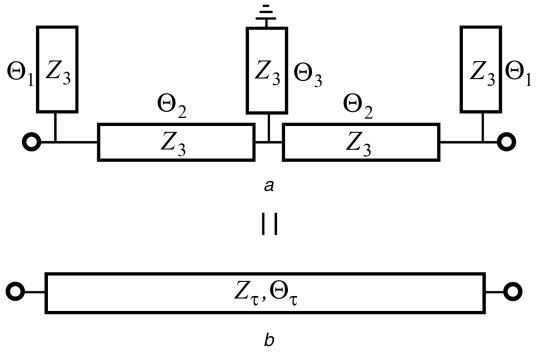

Fig. 5 *Conventional equivalent circuit to achieve the desired filtering response [3, Fig. 2]*
(a) Equivalent circuit for the filtering responses in [3], ***(b)*** Equivalent uniform TL with the characteristic impedance of Z_τ and electrical length of Θ_τ

Table 1 Design parameters of conventional BUPD [3]

	Θ_1, °	Θ_2, °	Θ_3, °	Z_τ, Ω	Θ_τ, °
group 1	79.4	8.96	2	50.12	89.93
group 2	75.18	11.86	4	50.32	90.66
group 3	72	13.77	6	50.07	89.76
design I	76.9	10.7	3.5	46.56	94.36

The equivalent circuit shown in Fig. 5*a*, that achieves the desired filtering response, is symmetric and, therefore, can be equivalent to a uniform TL with the assumed characteristic impedance of Z_τ and electrical length of Θ_τ in Fig. 5*b*. The even- and odd-mode admittances of the equivalent circuit in Fig. 5*a* are

$$Y_e = jY_3\tan\Theta_1 - jY_3\frac{(Y_3/2)\cot\Theta_3 - Y_3\tan\Theta_2}{Y_3 - (Y_3/2)\cot\Theta_3\tan\Theta_2} \tag{22a}$$

$$Y_o = jY_3(\tan\Theta_1 - \cot\Theta_2) \tag{22b}$$

where $Y_3 = Z_3^{-1}$.

Those of the equivalent uniform TL in Fig. 5*b* are

$$Y_{e\_TL} = jY_\tau\tan(\Theta_\tau/2) \tag{23a}$$

$$Y_{o\_TL} = -jY_\tau\cot(\Theta_\tau/2) \tag{23b}$$

where $Y_\tau = Z_\tau^{-1}$

From the relations in (22a), (22b) and (23a) and (23b), the design formulas for the characteristic impedance of Z_τ and the electrical length of Θ_τ are derived as

$$Z_\tau = (\sqrt{Y_eY_o})^{-1} \tag{24a}$$

$$\tan(\Theta_\tau/2) = \sqrt{\frac{-Y_e}{Y_o}} \tag{24b}$$

Substituting the first, second, and third rows of design parameters into the expressions in (24a) and (24b) gives around $Z_\tau = 50\,\Omega$ and $\Theta_\tau = 90°$ as listed in Table 1, by which it can be concluded that the design parameters given in [3] are the same as those calculated by (7a)–(7c) and (10a)–(10c) only under the conditions of equal power

Table 2 Design Parameters for $k^2 = 6$ and 4 dB

$k^2 = 6$ dB: $R_a = 40\,\Omega$, $R_b = 50\,\Omega$, $R_c = 60\,\Omega$ and $R_{ic} = 20\,\Omega$				
Z_{B0}	Z_{B1}	Z_{i1}	Z_{i2}	Z_{B2}
30 Ω	35.37 Ω	70.58 Ω	38.75 Ω	77.31 Ω
$k^2 = 4$ dB: $R_a = 60\,\Omega$, $R_b = 40\,\Omega$, $R_c = 50\,\Omega$ and $R_{ic} = 30\,\Omega$				
Z_{B0}	Z_{B1}	Z_{i1}	Z_{i2}	Z_{B2}
50 Ω	40.96 Ω	64.92 Ω	45.79 Ω	72.58 Ω

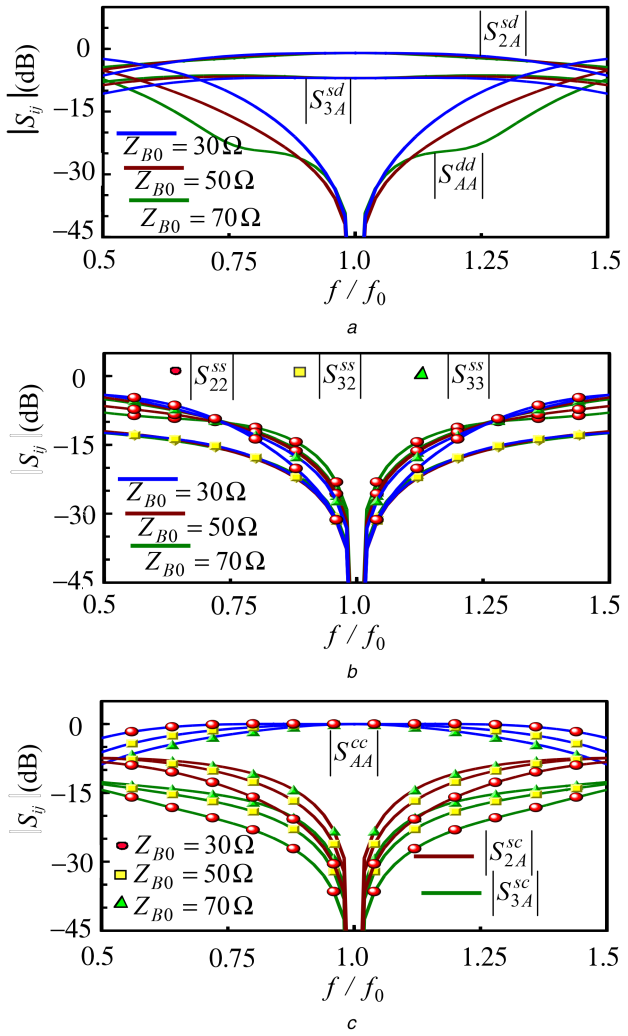

Fig. 6 *Frequency responses for* $k^2 = 6$ dB *for different values of* Z_{B0}, *(a)* $|S_{AA}^{dd}|$, $|S_{2A}^{sd}|$ and $|S_{3A}^{sd}|$, *(b)* $|S_{23}^{ss}|$, $|S_{22}^{ss}|$ and $|S_{33}^{ss}|$, *(c)* $|S_{AA}^{cc}|$, $|S_{2A}^{sc}|$ and $|S_{3A}^{sc}|$

division and equal termination impedances of 50 Ω. By the fourth design set in Table 1, however, $Z_\tau = 46.56\,\Omega$ and $\Theta_\tau = 94.4°$ are calculated as listed. Due to the phase delay of $\Theta_\tau = 94.4°$, thus being not 90°, an additional open stub l_5 [3, Fig. 17] is necessary for correcting the isolation deviation.

Reference [6] is also valid for equal power divisions and equal termination impedances. Reference [11] is valid for arbitrary power division ratios but effective only for equal termination impedances. Substituting $R_a = R_b = R_c = Z_0$ into [11, (17)], the same design formulas in (7a)–(7c) and (10a)–(10c) can be obtained.

The conventional work [7] is also valid only for the equal power divisions and for the equal termination impedances, and the design parameters of three prototypes are written in [7, Table 1]. For the first prototype, the *T*-type isolation circuit in Fig. 3*c* is employed with the values of $R_{ic} = 100\,\Omega$ and $Z_{i1} = Z_{i2} = 100\,\Omega$. Substituting $R_{ic} = 100\,\Omega$, $k = 1$ and $R_a = R_b = R_c = 50\,\Omega$ into (10a)–(10c), $Z_{i1} = Z_{i2} = 100\,\Omega$ can be calculated. For [7, Fig. 2], the two TLs with Z_{B1} and Z_{B2} in Fig. 1 are replaced with two identical 90° DC blocks with the even- and odd-mode impedances of Z_{e1} and Z_{o1}. In this case, the characteristic impedance of the coupled TL sections should be $(Z_{e1} - Z_{o1})$ /2 [23, (1)], [24] resulting in the same design parameters as those in (7a)–(7c) and (10a)–(10c). Those for the other two topologies [7, Figs. 5 and 7] are also the same as those from (7a)–(7c) and (10a)–(10c), as well.

The one in [12] is effective for arbitrary power divisions and for impedance transforming. Substituting $R_b = R_c$ into [12, (4)] gives the same design formulas and the *T*-type isolation circuit in Fig. 3*c* is employed as well. However, impedance-transforming function is verified only for equal power division.

2.5 Frequency responses

To verify the design formulas in (7a)–(7c), (10a)–(10c) and the scattering parameters in (21), two sets of design parameters were chosen depending on arbitrary power division ratios and arbitrary termination impedances. The first set is for $k^2 = 6$ dB, $R_a = 40\,\Omega$, $R_b = 50\,\Omega$ and $R_c = 60\,\Omega$, while the second set is for $k^2 = 4$ dB, $R_a = 60\,\Omega$, $R_b = 40\,\Omega$ and $R_c = 50\,\Omega$. For the isolation circuit, the *T*-type with a shunt resistor in Fig. 3*c* was employed. As mentioned previously in (7c) and (10c), the characteristic impedance of Z_{B0} and the isolation resistors of R_{ic} can be determined arbitrarily and, therefore, many sets of design parameters are available, two of which ($k^2 = 6$ and 4 dB) are listed in Table 2.

Based on the design parameters with $k^2 = 6$ dB in Table 2, varying the characteristic impedance values of Z_{B0} from 30 to 70 Ω and fixing $R_{ic} = 20\,\Omega$, the frequency responses are plotted in Fig. 6 where f_0 and f are the design and the operation frequencies, respectively. The frequency responses of the mixed scattering parameters can be generated by using the relations in (18a)–(18c) to (20) with the aid of any circuit simulator like advanced design system (ADS), and those of the scattering parameters of $|S_{AA}^{dc}|$ and $|S_{AA}^{cd}|$ in (20) will not be treated throughout this paper due to no important meaning. The frequency responses of $|S_{AA}^{dd}|$, $|S_{2A}^{sd}|$ and $|S_{3A}^{sd}|$ are plotted in Fig. 6*a* and those of $|S_{32}^{ss}|$, $|S_{22}^{ss}|$ and $|S_{33}^{ss}|$ in Fig. 6*b*, while those of $|S_{AA}^{cc}|$, $|S_{2A}^{sc}|$ and $|S_{3A}^{sc}|$ in Fig. 6*c*. The values of $|S_{AA}^{dd}|$ in Fig. 6*a* are all < -80 dB at f_0, regardless of the characteristic impedances values of Z_{B0}, and the widest bandwidth is shown when $Z_{B0} = 70\,\Omega$.

The scattering parameters of $|S_{2A}^{sd}|$ and $|S_{3A}^{sd}|$ in Fig. 6*a* are $|S_{2A}^{sd}| = -3.98$ dB and $|S_{3A}^{sd}| = -9.98$ dB at f_0, leading to the desired design power division ratio of 6 dB. The matching at the unbalanced ports ② and ③ and the isolation values are not influenced by either balanced or common mode. Near-perfect matching at ports ② and ③, and near-perfect isolations between them are achieved at f_0 for any value of Z_{B0} as demonstrated in Fig. 6*b* where the isolation responses are about the same even with different values of Z_{B0}. In the case of different termination impedance values of R_b and R_c for $k^2 = 6$ dB, the matching performance at port ③ is slightly better than that at port ②, because the difference between $2R_a$ and R_c is smaller than those between $2R_a$ and R_b. The frequency responses due to the common mode are shown in Fig. 6*c*. The values of $|S_{AA}^{cc}|$ are all 0 dB at f_0, and the power transmission scattering parameters of $|S_{2A}^{sc}|$ and $|S_{3A}^{sc}|$ are all < -120 dB at f_0, implying no power transfer from the common ports *A* to port ② or ③ with the common-mode excitation.

Another set of simulations was carried out for $k^2 = 4$ dB in Table 2 varying the isolation impedance values of R_{ic} from 30 to 70 Ω and fixing $Z_{B0} = 50\,\Omega$. The frequency responses of $|S_{AA}^{dd}|$, $|S_{2A}^{sd}|$ and $|S_{3A}^{sd}|$ are plotted in Fig. 7*a*, and those of $|S_{32}^{ss}|$, $|S_{22}^{ss}|$ and $|S_{33}^{ss}|$ in Fig. 7*b*, while those of $|S_{AA}^{cc}|$, $|S_{2A}^{sc}|$ and $|S_{3A}^{sc}|$ in Fig. 7*c*. A near-perfect matching at the balanced common port can be achieved at f_0, and the scattering parameters of S_{2A}^{dd} and S_{3A}^{dd} are -1.455 and -5.455 dB at f_0, respectively, leading the desired 4 dB power division ratio. Quite differently from the cases for $k^2 = 6$ dB in Fig. 6 generated

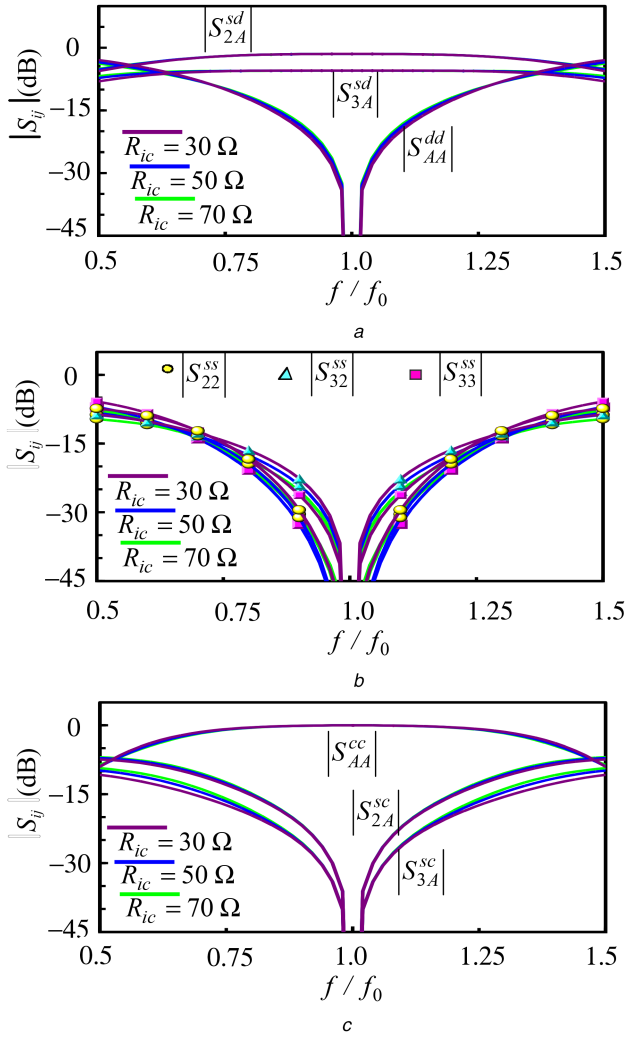

Fig. 7 *Frequency responses for* $k^2 = 4$ dB
(a) $|S^{dd}_{AA}|$, $|S^{sd}_{2A}|$ and $|S^{sd}_{3A}|$, ***(b)*** $|S^{ss}_{23}|$, $|S^{ss}_{22}|$ and $|S^{ss}_{33}|$, ***(c)*** $|S^{cc}_{AA}|$, $|S^{sc}_{2A}|$ and $|S^{sc}_{3A}|$

Table 3 Design and fabrication parameters

$k^2 = 5$ dB: $R_a = 60\ \Omega$, $R_b = 40\ \Omega$, $R_c = 50\ \Omega$ and $R_{ic} = 51\ \Omega$

Z_{B0}	Z_{B1}	Z_{i1}	Z_{i2}	Z_{B2}
50 Ω	39.74 Ω	92.15 Ω	57.93 Ω	79.02 Ω
$w = 1.56$	$w = 2.17$	$w = 0.54$	$w = 1.24$	$w = 0.73$
$\ell = 54.66$	$\ell = 27.05$	$\ell = 28.14$	$\ell = 27.52$	$\ell = 27.93$

unit; mm.

by varying the values of Z_{B0}, the frequency responses in Fig. 7 produced by varying the values of R_{ic} are about the same, a feature that may be used for the design parameters.

3 Measurements

For the verification of the suggested theory, one prototype terminated in $R_a = 60\,\Omega$, $R_b = 40\,\Omega$ and $R_c = 50\,\Omega$ was designed at $f_0 = 2$ GHz and fabricated on a substrate (RT/Duroid 5880, $\varepsilon_r = 2.2$, $H = 20$ mil) for the power division ratio of $k^2 = 5$ dB. In this case, the *IC* in Fig. 1 required two different resistors of $R_b = 40\,\Omega$ and $R_c = 50\,\Omega$ but not available for the off-the-shelf resistors (e.g. 0603 chip resistors). So, the *T*-type in Fig. 3*c* was employed where the resistance value of R_{ic} was arbitrarily selected as 51 Ω.

The design and fabrication parameters are collected in Table 3 where $Z_{B0} = 50\,\Omega$ was arbitrarily chosen, and the design values of Z_{B1}, Z_{i1}, Z_{i2}, and Z_{B2} were calculated as 39.74, 92.15, 57.93, and 79.02 Ω, respectively. The dimensions for w and ℓ are width and length of each TL. The fabricated prototype is displayed in Fig. 8

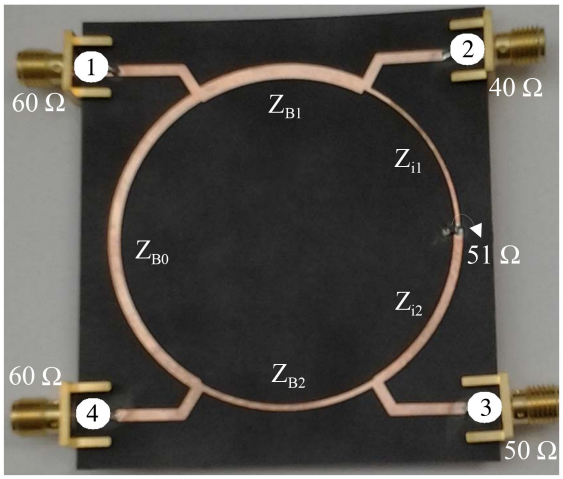

Fig. 8 *Fabricated prototype terminated in* $R_a = 60\,\Omega$, $R_b = 40\,\Omega$, $R_c = 50\,\Omega$

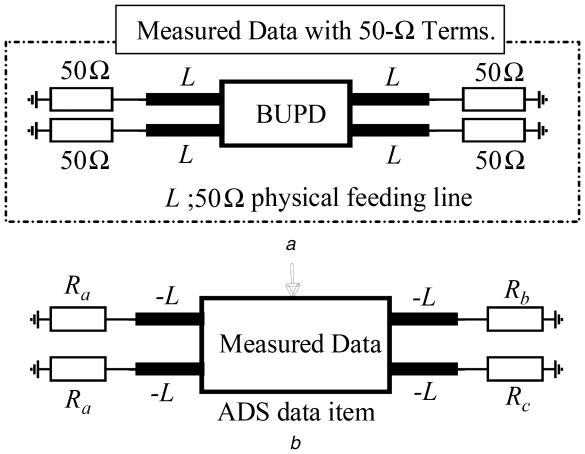

Fig. 9 *Measuring technique for non-50 Ω termination impedances*
(a) With 50-Ω termination impedances, ***(b)***A way to get measured data with non-50 Ω termination impedances of R_a, R_b and R_c

where the termination impedance and the characteristic impedance of each feeding line are 50 Ω for the measurements, even with $R_a = 60\,\Omega$, $R_b = 40\,\Omega$ and $R_c =$ Ω. It was measured in the form in Fig. 9*a* with the 50-Ω feeding lines having each physical length L.

The measured scattering parameters can be changed with the termination impedances but the measured circuit parameters like admittance, impedance and *ABCD* parameters are kept unchanged regardless of the termination impedances. The measured data including the feeding line effect are, as demonstrated in Fig. 9*b*, saved in ADS data item. To remove the feeding line effect, connect a 50-Ω feeding line with the physical length of $-L$ to each port and terminate the port termination impedances of R_a, R_b, and R_c. If the ADS data item is simulated once more with the desired termination impedances, the wanted measured frequency responses can be obtained.

The measured frequency responses are compared with the predicted ones in Fig. 10 where solid lines are the measured responses, while dotted ones for the predicted ones. The frequency responses of $|S^{dd}_{AA}|$, $|S^{sd}_{2A}|$ and $|S^{sd}_{3A}|$ are plotted in Fig. 10*a*, those of $|S^{ss}_{23}|$, $|S^{ss}_{22}|$ and $|S^{ss}_{33}|$ in Fig. 10*b*, while those of $|S^{cc}_{AA}|$, $|S^{sc}_{2A}|$ and $|S^{sc}_{3A}|$ in Fig. 10*c*. At 2 GHz, the measured values of $|S^{dd}_{AA}|$, $|S^{sd}_{2A}|$, and $|S^{sd}_{3A}|$ in Fig. 10*a* are −27.87, −1.27, and −6.18 dB, respectively, leading the power division ratio of 4.91 dB. Those of $|S^{ss}_{23}|$, $|S^{ss}_{22}|$, and $|S^{ss}_{33}|$ in Fig. 10*b* are −27.68, −29.87, and −27.70 dB, respectively. Those of $|S^{cc}_{AA}|$, $|S^{sc}_{2A}|$, and $|S^{sc}_{3A}|$ in Fig. 10*c* are −0.18, −34.75, and −34.87 dB, respectively. The measured responses are in good agreement with the predicted ones.

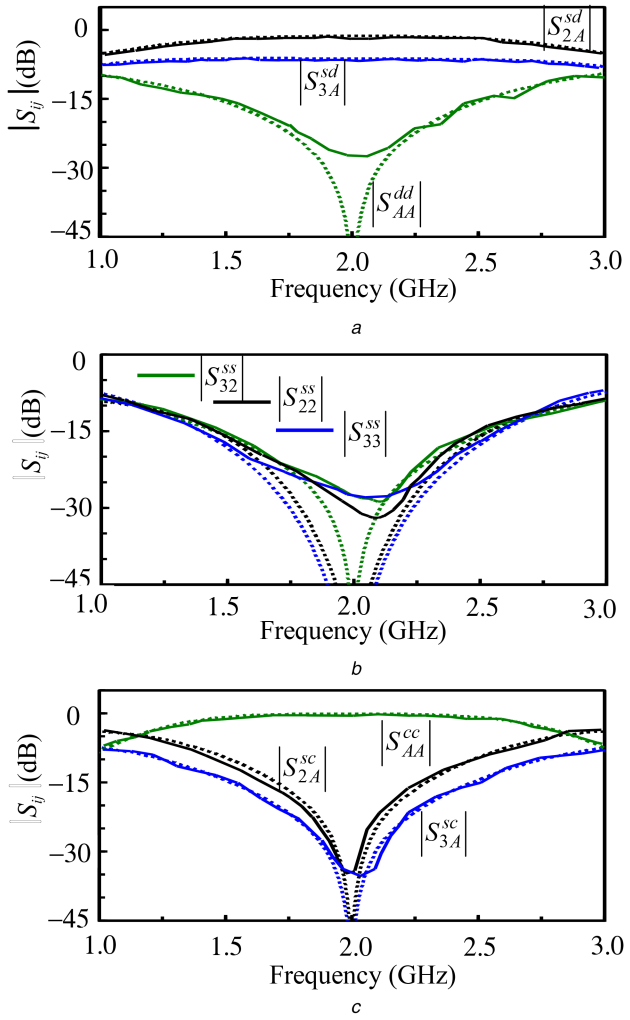

Fig. 10 *Measured frequency responses (solid lines) are compared with the predicted ones (dotted lines) for the prototype*
(a) $|S^{dd}_{AA}|$, $|S^{sd}_{2A}|$ and $|S^{sd}_{3A}|$, ***(b)*** $|S^{ss}_{23}|$, $|S^{ss}_{22}|$ and $|S^{ss}_{33}|$, ***(c)*** $|S^{cc}_{AA}|$, $|S^{sc}_{2A}|$ and $|S^{sc}_{3A}|$

4 Conclusions

Here, the BUPDs were suggested for the arbitrary power division ratios and for the arbitrary real termination impedances. It consists of one 180° TL, two 90° TLs and an *IC* but due to arbitrary termination impedances, no symmetric line was available, requiring complicated full-port analyses. To make the design process simpler, two equivalent circuits were derived under the assumption of the perfect isolation, based on which the design formulas were successfully derived.

Since the suggested BUPDs can function as not only balanced power dividers but also impedance transformers, they can be expected to be utilised for the diverse applications requiring compact size in microwave integrated circuits.

5 References

[1] Xia, B., Wu, L.-S., Mao, J.: 'A new balanced-to-balanced power divider/combiner', *IEEE Trans. Microwave Theory Techn.*, 2012, **60**, pp. 2791–2798

[2] Feng, W., Che, W., Xue, Q.: 'Wideband in-phase and out-of-phase balanced power dividing and combining networks', *IEEE Trans. Microwave Theory Techn.*, 2014, **62**, pp. 1192–1202

[3] Xu, K., Shi, J., Lin, L., *et al.*: 'A balanced-to-unbalanced microstrip power divider with filtering function', *IEEE Trans. Microwave Theory Techn*, 2015, **63**, pp. 2561–2569

[4] Shi, J., Wang, J., Xu, K., *et al.*: 'A balanced-to-balanced power divider with wide bandwidth', *IEEE Microw. Wireless Compon.Lett.*, 2015, **25**, (9), pp. 573–575

[5] Feng, W., Zhao, C., Che, W., *et al.*: 'Wideband balanced network with high isolation using double-sided parallel-strip line', *IEEE Trans. Microwave Theory Techn*, 2015, **63**, (12), pp. 4013–4018

[6] Li, L., Cheng, W., Wu, L.-S., *et al.*: 'A wideband filtering balance-to-unbalanced out-of-phase power divider', *IEEE Microw. Wireless Compon.Lett.*, 2018, **28**, (10), pp. 870–872

[7] Gao, X., Feng, W., Che, W., *et al.*: 'Wideband balanced-to-unbalanced filtering power dividers based on coupled lines', *IEEE Trans. Microwave Theory Tech.*, 2017, **65**, (1), pp. 86–95

[8] Shi, J., Lu, J., Xu, K., *et al.*: 'A coupled-line balanced-to-single-ended out-of-phase power divider with enhanced bandwidth', *IEEE Trans. Microwave Theory Tech.*, 2017, **65**, (2), pp. 459–466

[9] Xia, B., Wu, L.-S., Ren, S.-W., *et al.*: 'A balanced-to-balanced power divider with arbitrary power division', *IEEE Trans. Microwave Theory Techn*, 2013, **61**, pp. 2831–2840

[10] Feng, W., Zhao, C., Che, W., *et al.*: 'A balanced-to-balanced network with unequal power division and wideband common mode suppression', *IEEE Microw. Wireless Compon.Lett.*, 2016, **26**, (4), pp. 237–239

[11] Yadav, A. N., Bhattacharjee, R.: 'Balanced to unbalanced power divider with arbitrary power ratio', *IEEE Microw. Wireless Compon. Lett.*, 2016, **26**, (11), pp. 885–887

[12] Zhuang, Z., Wu, Y., Kong, M., *et al.*: 'Dual-band filtering balanced-to-unbalanced impedance-transforming power divider with high frequency ratio and arbitrary power division', *IEEE. Access.*, 2018, **6**, pp. 12710–12717

[13] Ahn, H.-R., Chang, I.-S., Yun, S.-W.: 'Miniaturized 3-dB ring hybrid terminated by arbitrary impedances', *IEEE Trans. Microwave Theory Tech.*, 1994, **42**, pp. 2216–2221

[14] Ahn, H.-R., Wolff, I., Chang, I.-S.: 'Arbitrary termination impedances, arbitrary power division, and small-sized ring hybrids', *IEEE Trans. Microwave Theory Tech.*, 1997, **45**, pp. 2241–2247

[15] Ahn, H-R., Wolff, I.: 'Asymmetric four-port and branch-line hybrids', *IEEE Trans. Microwave Theory Tech.*, 2000, **48**, pp. 1585–1588

[16] Sun, Z., Zhang, L., Yan, Y., *et al.*: 'Design of unequal dual-band gysel power divider with arbitrary termination resistance', *IEEE Trans. Microwave Theory Tech.*, 2011, **59**, pp. 1955–1962

[17] Tripathi, V. K., Chin, Y.K.: 'Analysis of the general nonsymmetrical directional coupler with arbitrary terminations'. IEE Proc. H. Microwaves, Optics and Antennas, col. 129, 1982, pp. 360–362

[18] Ahn, H.-R.: '*Asymmetric passive components in microwave integrated circuits*' (Wiley, New York, 2006) Chap. 2

[19] Ahn, H.-R., Wolff, I.: 'General design equations, small-sized impedance transformers, and their applications to small-sized three-port 3–dB power dividers', *IEEE Trans. Microw. Theory Techn.*, 2001, **49**, pp. 1277–1288

[20] Ahn, H.-R.: 'Modified asymmetric impedance transformers (MCVTs and MCCTs) and their applications to impedance-transforming three-port 3–dB power dividers', *IEEE Trans. Microw. Theory Techn.*, 2011, **59**, pp. 3312–3321

[21] Ahn, H.-R., Itoh, T.: 'New isolation circuits of compact impedance-transforming 3-dB baluns for theoretically perfect isolation and matching', *IEEE Trans. Microw. Theory Techn.*, 2010, **58**, pp. 3892–3902

[22] Ahn, H.-R., Kim, B.: 'Toward integrated size reduction', *IEEE Microw. Mag.*, 2008, **9**, (1), pp. 65–75

[23] Ahn, H.-R., Tentzeris, M. M.: 'Wideband and compact impedance-transforming 90° DC blocks with symmetric coupled transmission-line sections', *IEEE Trans. Compon., Packag., Manuf. Technol.*, 2019, **9**, (1), pp. 80–87

[24] Ahn, H.-R., Itoh, T.: 'Impedance-transforming symmetric and asymmetric DC blocks', *IEEE Trans. Microw. Theory Techn.*, 2010, **58**, pp. 2463–2474